Lattice Dynamics of Terbium†

J. C. GLYDEN HOUMANN* AND R. M. NICKLOW

Solid State Division, Oak Ridge National Laboratory, Oak Ridge, Tennessee 37830

(Received 19 November 1969)

The frequency–wave-vector dispersion relation for the normal modes of vibration of terbium at room temperature has been measured by means of slow-neutron inelastic scattering techniques. The triple-axis spectrometer at the Oak Ridge high flux isotope reactor was used, mostly in the constant-Q mode of operation. Phonon frequencies for wave vectors along the principal symmetry directions have been determined and, in addition, measurements of phonon frequencies along the boundaries of the Brillouin zone and along a more general direction are reported. The data have been fitted with a Born–von Kármán force model which includes interactions out to the eighth nearest neighbor. The interactions have been assumed to be general (tensor) out to the fourth neighbor and axially symmetric beyond. The model has been used to calculate a frequency distribution function $g(\nu)$ and related quantities such as the lattice specific heat and Debye temperature.

I. INTRODUCTION

RECENTLY, there has been much interest in the lattice dynamics of the heavy rare-earth metals in connection with magnon-phonon interactions observed[1-3] in the measured magnon dispersion relations of Tb and Tb–10 at.% Ho and with the calculation of thermodynamical properties.[4,5] However, only very little experimental information has previously been reported about the phonon energies in the rare earths,[6] and this information has not been used to investigate interatomic forces. Therefore, a systematic study of these materials has been initiated at the Oak Ridge National Laboratory.

In the present paper we report neutron inelastic scattering measurements of the phonon dispersion relation of Tb at room temperature. We have made complete measurements of the dispersion relation for the principal symmetry directions and have obtained considerable information about the phonon energies along the boundaries of the Brillouin zone.

The data have been analyzed by means of a Born–von Kármán interatomic force model, and the necessity of including zone-boundary data in the fitting in order to obtain a satisfactory model is emphasized. The model obtained from this analysis provides the basis for a calculation of a frequency distribution function for Tb, and this is in turn has been used to calculate a variety of thermodynamical properties. In particular, the lattice specific heat has been calculated as a function of temperature, and at 90°K, where a calculation of the mag-

netic specific heat exists,[5] the total calculated specific heat has been compared with experiment.[7]

II. MEASUREMENTS AND RESULTS

The measurements were carried out at the Oak Ridge high flux isotope reactor using a triple-axis spectrometer. The majority of the data was obtained with the "constant-Q" method,[8] although some high-resolution measurements were made in "mixed scans" in which both Q and E were varied in order to scan along a direction in the Q-E plane which is perpendicular to the dispersion relation. For most of the measurements, the analyzer was set to accept scattered neutrons with an energy E' corresponding to a frequency of 6×10^{12} cps (~ 24 meV), although in order to check the data, some measurements were carried out using scattered neutrons with frequencies of 3.5×10^{12}, 5×10^{12}, and 7.5×10^{12} cps. As monochromator and analyzer, the (0002) Bragg reflections from two Be crystals were used.

Two samples were used for the measurements. One was a cylindrical single crystal, 50 mm long and 6 mm in diameter. This crystal was grown by the zone-melting technique by Metals Research, and it was oriented with the c axis nearly along the crystal axis. All the measurements in the ab plane were made on this crystal. The second sample was a much larger disk-shaped crystal grown by the strain-anneal method by R. Reed of the ORNL Solid State Division. This crystal was used for the remainder of the measurements. For Tb at room temperature the lattice parameters are $a = 3.599$ Å and $c = 5.696$ Å.

Examples of several phonon peaks obtained in this study are shown in Fig. 1. Focusing[9-11] is strongly dependent on the dispersion-curve slope, as evidenced by Figs. 1(a) and 1(b). We have taken advantage of focus-

[1] H. Bjerrum Møller, J. C. Gylden Houmann, and A. R. Mackintosh, Phys. Rev. Letters **19**, 312 (1967).

[2] H. Bjerrum Møller, J. C. Gylden Houmann, and A. R. Mackintosh, J. Appl. Phys. **39**, 807 (1968).

[3] H. Bjerrum Møller, M. Nielsen, and A. R. Mackintosh, J. Appl. Phys. (to be published).

[4] L. J. Sundström, Ann. Acad. Sci. Fennicae **A VI 280**, 1 (1968).

[5] J. C. Gylden Houmann, in *Neutron Inelastic Scattering* (International Atomic Energy Agency, Vienna, 1968), Vol. II, p. 29.

[6] J. A. Leake, V. J. Minkiewicz, and G. Shirane, Solid State Commun. **7**, 535 (1969).

[7] L. D. Jennings, R. M. Stanton, and F. H. Spedding, J. Chem. Phys. **27**, 909 (1957).

[8] B. N. Brockhouse, in *Inelastic Scattering of Neutrons in Solids and Liquids* (International Atomic Energy Agency, Vienna, 1961), p. 113.

[9] M. F. Collins, Brit. J. Appl. Phys. **14**, 805 (1963).

[10] M. J. Cooper and R. Nathans, Acta Cryst. **23**, 357 (1967).

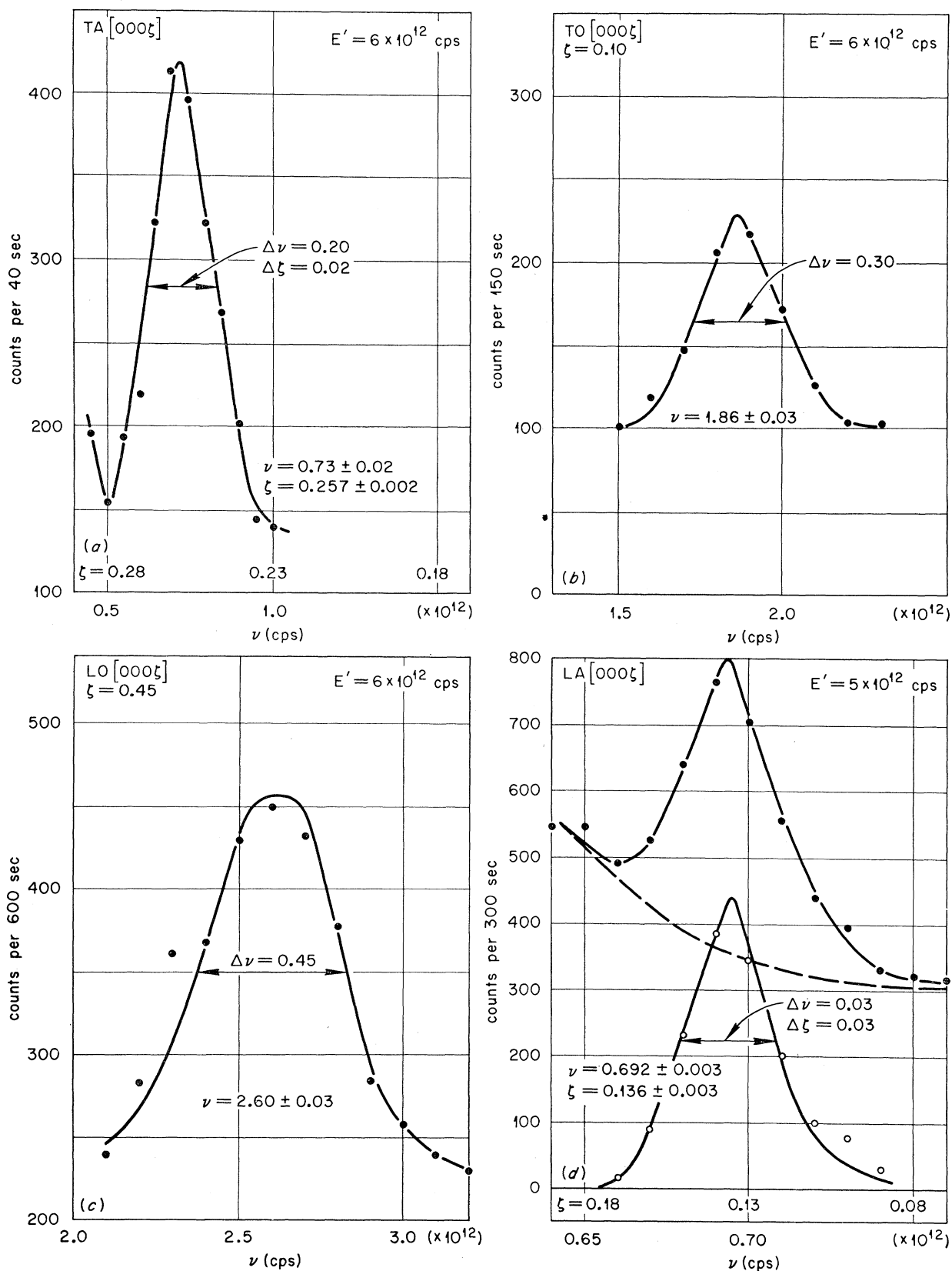[11] M. Nielsen and H. Bjerrum Møller, Acta Cryst. **A25**, 547 (1969).

FIG. 1. Several typical phonon peaks for Tb obtained in "constant-Q" and "mixed" scans.

FIG. 2. Phonon dispersion curves for Tb in the major symmetry directions at room temperature.
The lines shown represent the eighth-nearest-neighbor "mixed" force model (see text).

ing effects in a high-resolution study of the [0001] LA branch in a search for a Kohn anomaly (discussed later in this section), and Fig. 1(d) shows a typical neutron group obtained in this study. The broader peaks in Figs. 1(b) and 1(c) are typical for phonons measured near zone boundaries and other regions where the dispersion curve slope is very small or zero. The majority of the observed phonon peaks had widths and intensities between the extremes shown in Fig. 1, although some neutron groups obtained along the zone boundaries were less well defined.

A selection of measured phonon frequencies in Tb at room temperature is given in Table I, and the complete results are shown in Figs. 2 and 3. The experimental errors are generally smaller than 3% and are frequently

below 2%. Because of an unfortunate orientation of the crystal used for the zone-boundary measurements and the relatively high absorption cross section of Tb (45–70 b at the neutron energies used), we have not been able to obtain a complete set of data along the boundaries of the Brillouin zone and the data that have been obtained are present in Fig. 3.

In presenting the dispersion curves along all high-symmetry directions, namely, Σ, T, T', R, S, S', Δ, P, and U (see Fig. 4), we have classified them according to the allowable irreducible representations of the invariant subgroup of symmetry operations, which are associated with each high-symmetry direction and point. The notation of Raubenheimer and Gilat[12] has been used. The solid curves are the result of a nonlinear

FIG. 3. Phonon dispersion curves for Tb along the boundaries of the Brillouin zone at room temperature.
The lines shown represent the eighth-nearest-neighbor force model.

[12] L. J. Raubenheimer and G. Gilat, Phys. Rev. 157, 586 (1967).

TABLE I. Selection of measured normal mode frequencies (in units of 10^{12} cps) in Tb at room temperature.

Γ_6^-	1.82 ± 0.03	Γ_3^+	3.25 ± 0.04
A_3	1.30 ± 0.02	A_1	2.44 ± 0.04
M_4^-	1.75 ± 0.03	M_4^+	1.59 ± 0.04
M_3^-	2.85 ± 0.05	M_3^+	2.90 ± 0.03
M_2^-	3.05 ± 0.04	M_1^+	2.89 ± 0.04
K_1	2.91 ± 0.06	K_2	2.86 ± 0.04
K_6	2.32 ± 0.04	K_5	2.35 ± 0.04
$L_1(A)$	1.78 ± 0.06	$L_1(0)$	3.13 ± 0.06
L_2	2.25 ± 0.06	H_3	1.38 ± 0.06

least-squares fit to the data for a Born–von Kármán interatomic force model to be discussed in Sec. III.

As will be discussed in Sec. III, it is not possible to determine all the parameters in this force model from the measurements along the high-symmetry directions and the zone edges, and therefore we have performed additional measurements along a more general direction, namely, $[\zeta \ \zeta \ -2\zeta \ \frac{1}{4}]$. These additional measurements which permit the evaluation of a complete set of parameters are shown in Fig. 5.

All the experimental results given here were obtained with Soller-slit collimators [full width at half-maximum (FWHM)$=0.6°$] both before and after the specimen. Where necessary, the data have been corrected for sloping backgrounds, but no other corrections have been applied. In particular, it has been assumed that the possible effect of the vertical resolution of the spectrometer on the long-wavelength modes (to produce a shift in the observed scattered-neutron peak towards
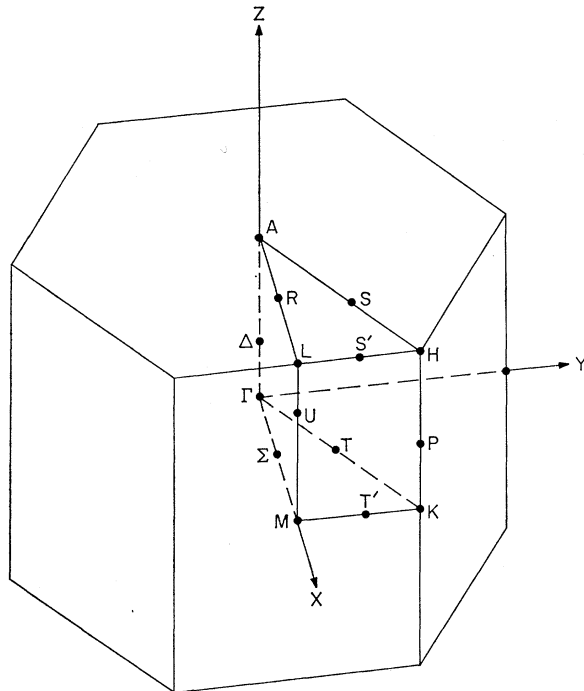
FIG. 4. First Brillouin zone for a hcp lattic. The irreducible zone is indicated in particular.

TABLE II. Dynamical matrix used in the analysis of Tb data.

Neighbor	Coordinates of typical atom	Force-constant matrix elements ϕ_{xy}		
1	$(a/\sqrt{3}, 0, \frac{1}{2}c)$	α_1	0	δ_1
		0	β_1	0
		δ_1	0	γ_1
2	$(0,a,0)$	α_2	ϵ_2	0
		$-\epsilon_2$	β_2	0
		0	0	γ_2
3	$(-2a/\sqrt{3}, 0, \frac{1}{2}c)$	α_3	0	δ_3
		0	β_3	0
		δ_3	0	γ_3
4	$(0,0,c)$	α_4	0	0
		0	α_4	0
		0	0	γ_4
5	$(5a/2\sqrt{3}, \frac{1}{2}a, \frac{1}{2}c)$			
6	$(a\sqrt{3}, 0, 0)$	$\phi_{xy}{}^n = (x_n y_n/R^2)(\phi_r{}^n - \phi_t{}^n) + \phi_t{}^n \delta_{xy}$		
7	$(0,a,c)$	$R = (x_n^2 + y_n^2 + z_n^2)^{1/2}$		
8	$(0, 2a, 0)$	$n = 5, 6, 7, \text{ or } 8$		

higher frequency) is negligible. The consistency of our data supports this assumption.

Tb possesses a spiral magnetic structure in a very narrow temperature range $(216–226°K)$,[13] and the wave vector $\mathbf{k}_0$ of the spiral is approximately 0.11 Å^{-1}.[14] This spiral structure is believed to be caused by a nesting of parallel sheets of the Fermi surface in the c direction that are separated by a distance $\mathbf{k}_0$.[15] Since this type of nesting can lead to Kohn anomalies in the phonon spectra for metals, it was thought that a Kohn anomaly might be observed in the c-direction dispersion relation for a wave vector $\mathbf{q}=0.11$ Å^{-1}. To search for such a Kohn anomaly, we have made very high-resolution measurements of the LA branch of the $[0001]$ direction near a $\mathbf{q}$ of 0.11 Å^{-1}. The measurements were performed around the $11\bar{2}4$ reciprocal-lattice point in order to take advantage of focusing effects. We were able to obtain very narrow and well-determined phonon peaks [an example of such a peak is shown in Fig. 1(d)]. Unfortunately, because of contamination from other phonon branches and from elastic scattering, we were able to carry out these measurements only in a very narrow $\mathbf{q}$ range around $\mathbf{q}=\mathbf{k}_0$. Although there is some evidence of a very small Kohn anomaly in the data, we do not at the present time have enough information to state that a Kohn anomaly has definitely been observed. Holmium, which also has a stable spiral magnetic structure, may make a much better candidate for a search for a Kohn anomaly. The effect could be larger since the spiral structure is stable over a very wide temperature range. The phonon dispersion relation for Ho is presently being studied.

[13] O. W. Dietrich and J. Als-Nielsen, Phys. Rev. 162, 315 (1967).
[14] W. C. Koehler, H. R. Child, E. O. Wollan, and J. W. Cable, J. Appl. Phys. 34, 1335 (1963).
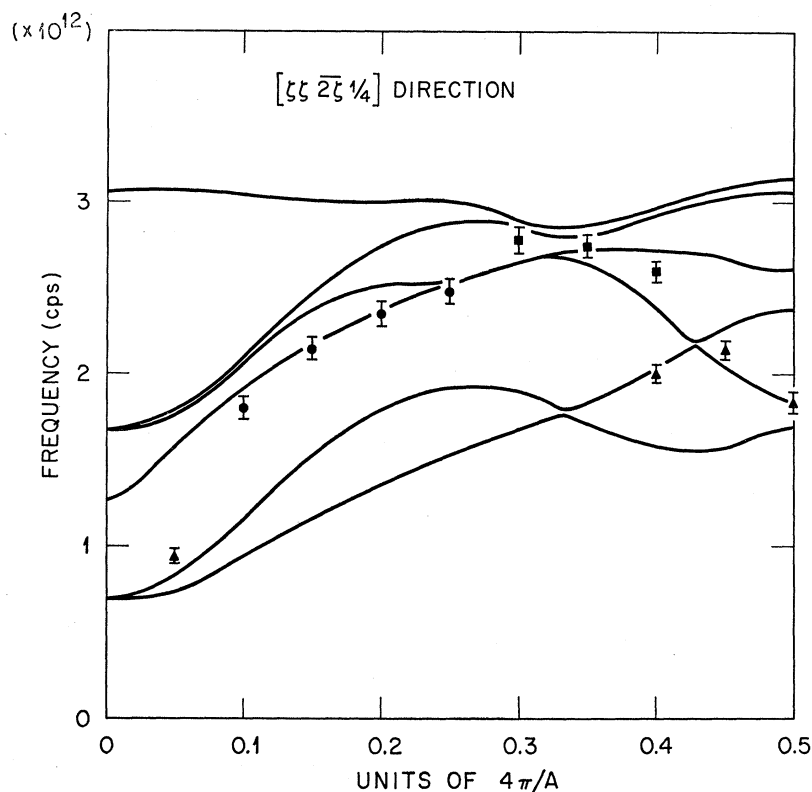[15] S. C. Keeton and T. L. Loucks, Phys. Rev. 168, 672 (1968).

FIG. 5. Phonon dispersion curves for Tb along the $[\zeta\ \zeta\ -2\zeta\ \frac{1}{4}]$ direction at room temperature. The lines shown represent the eighth-nearest-neighbor force model.

III. THEORETICAL CALCULATIONS

A. Model

The data have been fitted with a Born–von Kármán atomic force model. The model we have used is actually a "mixed" model that includes general (tensor) interactions out to fourth nearest neighbors and axially symmetric interactions starting with the fifth nearest neighbors. Table II gives the form of the dynamical matrix used in the analysis. We find that at least an eight-neighbor model is needed in order to obtain a satisfactory fit to all the data. The solid lines in Figs. 2, 3, and 5 show the fit obtained with this model and in Table III are given the values obtained for the inter-atomic force constants.

In the least-squares fitting procedure it is extremely important to utilize the zone-boundary data, since the parameters δ_1 and δ_3 (related to the x-z part of the first- and third-neighbor interactions) do not enter in the expression for the dispersion relation in the principal high-symmetry directions. These parameters are comparable in size to the remaining parameters, and they are essential for obtaining a good fit to the zone-boundary data. Furthermore, the parameters for the first three neighbors derived from this model strongly violate the restrictions that would be imposed by axially symmetric or modified axially symmetric interactions.[16] For example, both interactions restrict $\delta_1 = \frac{1}{2}\sqrt{3}\gamma(\alpha_1-\beta_1)$,

[16] R. E. DeWames, T. Wolfram, and G. W. Lehman, Phys. Rev. 138, A717 (1965).

where γ is the c/a ratio. This restriction would yield a value of 5350 dyn/cm compared to the fitted value of 7286 dyn/cm.

TABLE III. Best-fit eighth-nearest-neighbor forces model.

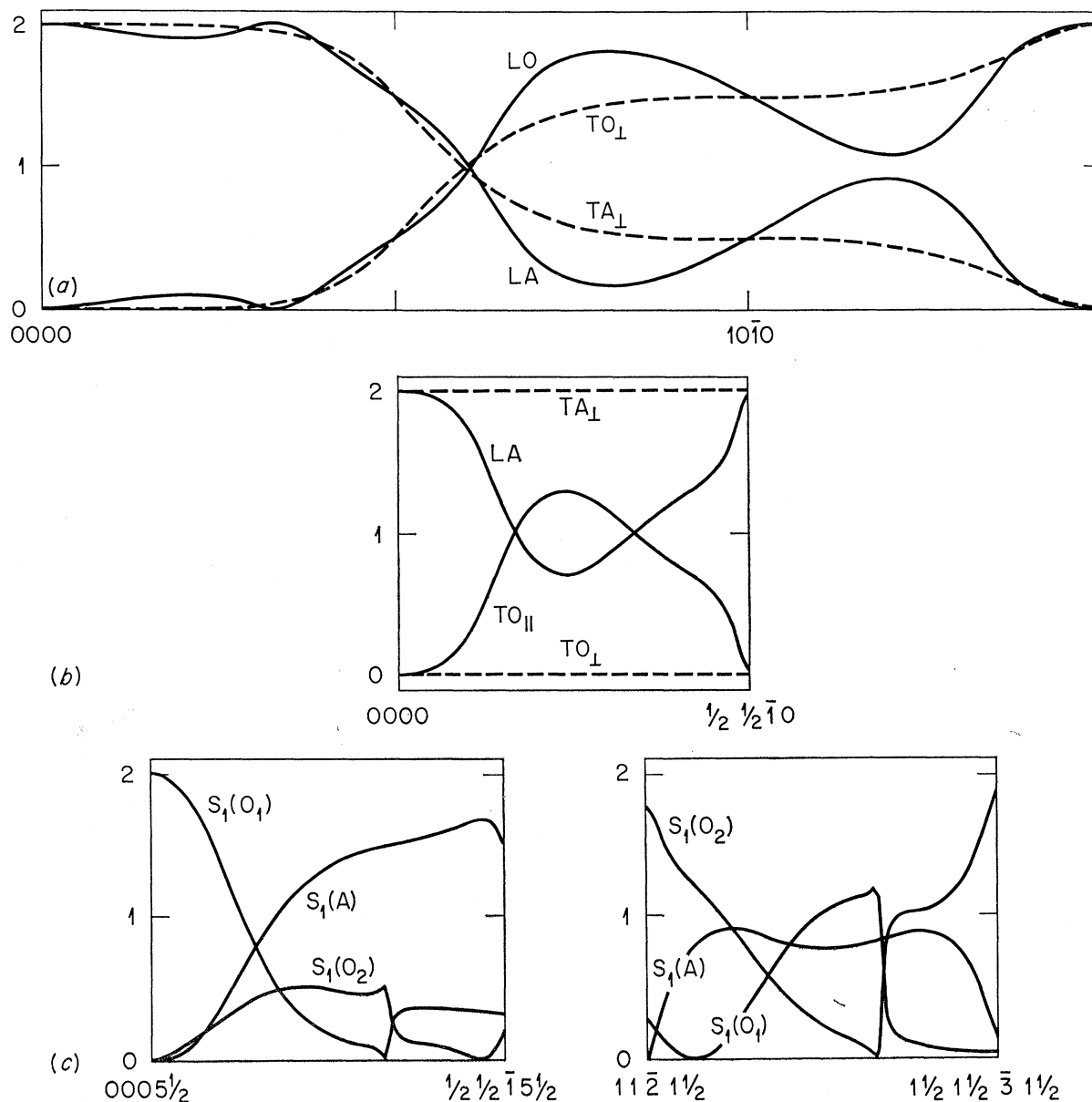| Neighbor		Force constants (dyn/cm)
1	α_1	5467
	β_1	1562
	γ_1	9901
	δ_1	7286
2	α_2	954
	β_2	11416
	γ_2	−952
	ϵ_2	2426
3	α_3	−1889
	β_3	−975
	γ_3	−894
	δ_3	46
4	α_4	−32
	γ_4	−2228
5	ϕ_r^5	1225
	ϕ_t^5	−180
6	ϕ_r^6	1250
	ϕ_t^6	241
7	ϕ_r^7	762
	ϕ_t^7	−98
8	ϕ_r^8	−410
	ϕ_t^8	66

FIG. 6. Inelastic structure factor curves for various branches of the phonon spectrum, calculated on the basis of the eighth-nearest-neighbor model. (a) $[10\bar{1}0]$ direction LA, LO, TA$_\perp$, and TO$_\perp$; (b) $[11\bar{2}0]$ direction LA, TO$_{\text{II}}$, TA$_\perp$, and TO$_\perp$; (c) AHL direction.

By fitting to the symmetry data alone, it is possible only to determine $\phi_r{}^7 - \phi_t{}^7$ for the seventh neighbor, and in order to obtain a complete set of parameters we have performed additional measurements along the more general direction $[\zeta\,\zeta\,-2\zeta\,\tfrac{1}{4}]$ (see Fig. 5). The inclusion of these data in the fitting does not provide a model which gives a significantly better over-all fit to the high-symmetry data. The result is consistent with the fact that $\phi_t{}^7$ is small compared with the dominant parameters. The other tangential parameters of this model are also generally an order of magnitude smaller than the radial parameters.

This is, to our knowledge, the first attempt to include zone-boundary measurements in the least-squares-fitting procedure for a hexagonal structure. Since these data are essential for determining the parameters of this model, it is probably justified to question the adequacy of previously obtained models for hexagonal materials.[17-20]

[17] P. K. Iyengar, G. Venkatoraman, P. R. Vijayaraghavan, and A. P. Roy, in *Inelastic Neutron Scattering* (International Atomic Energy Agency, Vienna, 1965), Vol. I, p. 153.
[18] G. L. Squires, Proc. Phys. Soc. (London) **88**, 919 (1966).
[19] R. E. Schmunk, Phys. Rev. **149**, 450 (1966).
[20] G. Borgonovi, G. Caglioti, and J. J. Antal, Phys. Rev. **132**, 683 (1963).
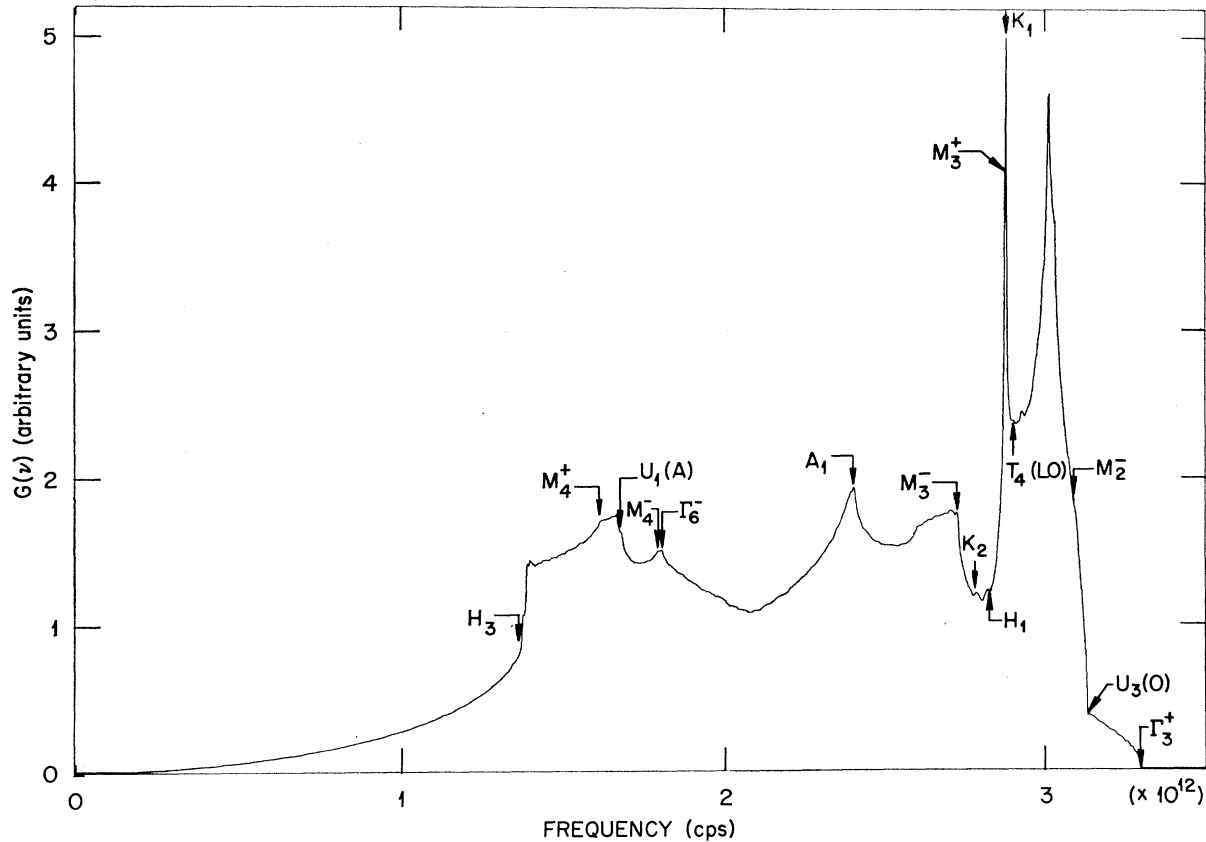
Tb G(ν) From 8-Neighbor Model fit to Inelastic Neutron Scattering Data.

FIG. 7. Unsmoothed computer plot of phonon frequency distribution function for Tb.
Indicated critical points are predicted from dispersion curves in Figs. 2 and 3.

We obtained the best values of the model parameters by means of a nonlinear least-squares-fitting program written for the IBM-360/91 computer at ORNL. Nonlinear least-squares fitting is complicated in that there can exist numerous minima in the parameter space, and it is necessary to find the lowest minimum. In order to be reasonably sure that we have arrived at the best fit, we have made numerous calculations starting with different initial values of the parameters. Furthermore, the squares of the frequencies from certain pairs of branches in the high-symmetry directions can be added (e.g., $\nu_{LO}^2 + \nu_{LA}^2$ along Σ) to yield expressions which are linear in some of the force constants which occur in the second-, fourth-, and sixth-nearest-neighbor interactions.[21] Good initial estimates for these parameters, therefore, can be obtained by a linear fitting analysis. Such a linear analysis also yields a relatively unambiguous indication of the range of the interactions which the model must have to obtain a satisfactory fit to the entire data. We have carried out these linear analyses and feel reasonably sure that the model we present here is the best obtainable.

From the eighth-neighbor model in Table III, we have calculated the elastic constants. These are given in Table IV. We have compared the longitudinal and shear velocity of sounds for the c direction yielded by these elastic constants with the experimentally obtained results[22] and have found very good agreement. Moreover, within the experimental uncertainty, our data satisfy the rotational invariance requirement. That is, the initial slopes of the $TA_\perp$ branches in the [10$\bar{1}$0] and [11$\bar{2}$0] directions and the TA branch in the [0001] direction are the same. Although the data satisfy the requirement, a model fitted to the data may not, and therefore this particular restriction was imposed on the fitted model.

TABLE IV. Elastic constants for Tb calculated from eight-neighbor model (units: 10^{11} dyn/cm²).

$C_{11} = 7.38$	$C_{44} = 2.31$
$C_{33} = 8.00$	$C_{66} = 2.04$

[21] S. K. Sinha (private communication).

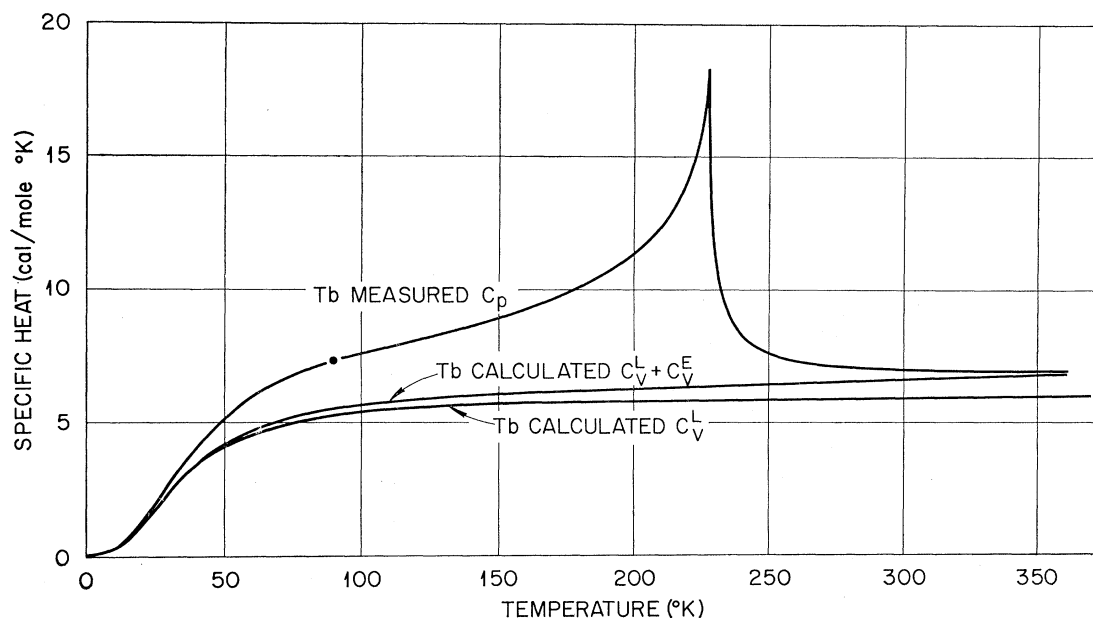[22] R. J. Pollina and B. Luthi, Phys. Rev. 177, 841 (1969).

FIG. 8. Measured specific heat (Ref. 7) and calculated lattice and electronic specific heats for Tb.

B. Calculations from Model

1. Inelastic structure factor. The intensity of coherent one-phonon scattering of slow neutrons, under the conditions of a constant-Q scan over the jth mode, in the case of phonon creation, is given by[23,24]

$$J_j = (h/4\pi)(k'/k_0)(n_j+1)e^{-2W}g_j{}^2(\mathbf{q},\tau), \qquad (1)$$

where $n_j = [\exp(h\nu_j/k_BT)-1]^{-1}$, k' and k_0 are the wave vectors of the scattered and incoming neutrons, respectively, W is the Debye-Waller factor, and $g_j{}^2$ is the inelastic structure factor given as

$$g_j{}^2(\mathbf{q},\tau) = \frac{b^2}{m\nu_j(\mathbf{q})}|\sum_s \boldsymbol{\xi}_{sj}\cdot\mathbf{Q}\exp(2\pi i\tau\cdot\mathbf{r}_s)|^2, \qquad (2)$$

where b is the coherent scattering length and m is the atomic mass. $\boldsymbol{\xi}_{sj}$ is the normalized eigenvector of the sth atom in the unit cell in the jth mode of vibration and $\mathbf{r}_s$ is the position vector of the sth atom within the unit cell. We see that the inelastic structure factor may be calculated for any mode of vibration if we know the appropriate eigenvectors $\boldsymbol{\xi}_{sj}$. These may be obtained from the theoretical model. The results of a calculation of $g_j{}^2$ for several modes of vibrations and for several directions are shown in Figs. 6(a)–6(c). We have plotted the structure factors in units of $Q^2b^2/m\nu_j$ in contrast to most other calculations, since in general we do not have pure modes. That is, for wave vectors $\mathbf{q}$ along a symmetry direction the vectors $\boldsymbol{\xi}_{sj}$ for each s are not always parallel and hence cannot be conveniently ex-

pressed as a product of unit vectors $\hat{\boldsymbol{\xi}}_j$ and their magnitudes ξ_{sj}.

In Figs. 6(a) and 6(b), which show the structure factors for the $TA_\perp$, $TO_\perp$, LA, and LO modes in the $[10\bar{1}0]$ direction and the $TA_\perp$, $TO_\perp$, LA, and TO_{II} structure factors for the $[11\bar{2}0]$ direction, we see several interesting features. First, the LA and LO structure factors do not cross in the region between $10\bar{1}0$ and $\frac{3}{2}\,0\,-\frac{3}{2}\,0$ but split apart with the LO structure factor going to 2 at $\frac{3}{2}\,0\,-\frac{3}{2}\,0$. This result is in contrast to a similar calculation by Iyengar et al. for Mg.[17] Our measurements support these calculations in that at $\frac{3}{2}\,0\,-\frac{3}{2}\,0$ we do observe the optical branch and not the acoustical. This feature can be related to the fact that for $\mathbf{q}$ vectors near the zone boundary, there is considerable mixing of the LA- and LO-mode eigenvectors, giving rise to modes which are neither pure acoustic nor optic. A simple third-nearest-neighbor calculation shows that such mixing occurs when $\alpha_1 - 3\beta_1 + 3(\alpha_3 + \beta_3) < 0$, a condition which the Tb parameters satisfy, whereas those for Mg do not. In the $[11\bar{2}0]$ direction there is a strong mixing of the LA and TO_{II} modes. These modes belong to the same symmetry group and hence are not allowed to cross. The mixing gives rise to the strong variation in the LA, TO_{II} structure factors shown in Fig. 6(b).

In Fig. 6(c) are given some examples of structure factors for zone-boundary phonons. A very strong dependence on the wave vector $\mathbf{q}$ is evident, and since this dependence is very model dependent, it is important to have a good model in order to find suitable places in reciprocal space for zone-boundary measurements.

2. Frequency distribution function. This function has

[23] I. Waller and P. O. Fröman, Arkiv Fysik **4**, 183 (1952).
[24] A. D. B. Woods, W. Cochran, and B. N. Brockhouse, Phys. Rev. **119**, 980 (1960).
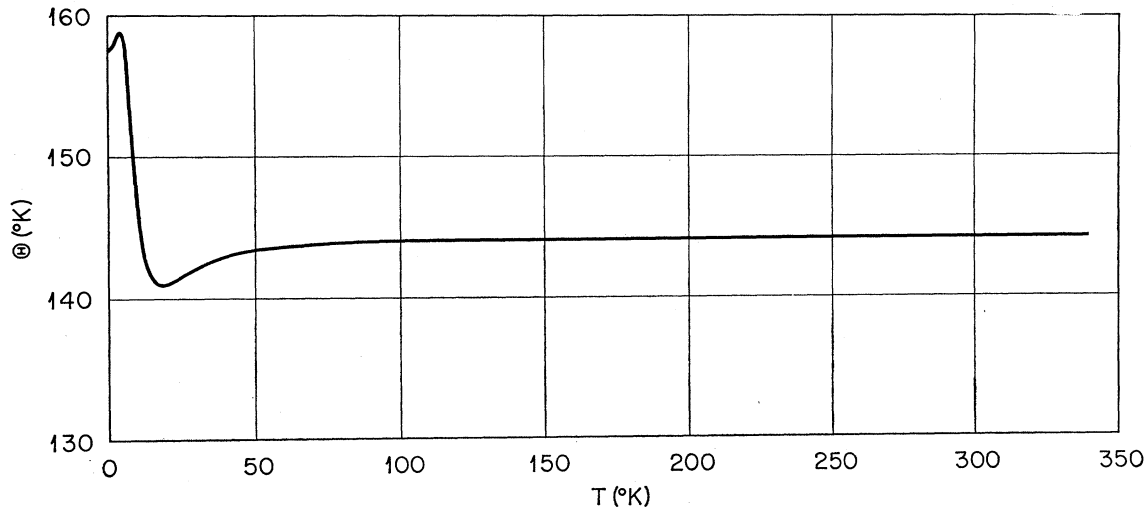
FIG. 9. Temperature dependence of the Debye temperature, derived from the lattice specific heat.

been computed using the method described by Rauben-heimer and Gilat,[12] appropriately modified for the more general Tb model. The frequencies, eigenvectors, and frequency gradients are calculated for a number (2100) of reduced wave vectors q_c, distributed within the irreducible 1/24 of the Brillouin zone (see Fig. 4). Assuming the gradients to be constant within small rectangular or triangular prisms surrounding a given q_c, the area of each frequency surface intersecting the prism is calculated. Summing over all modes and all prisms needed to fill the Brillouin zone, one obtains a very accurate representation of $g(\nu)$, as shown in Fig. 7. This figure is an unsmoothed computer plot, with the histogram of $g(\nu)d\nu$ sorted into about 1400 channels of $d\nu = 0.0025 \times 10^{12}$ cps. Critical points[25] expected from the dispersion curves are indicated. There are some critical points which cannot be predicted from the dis-persion relations in the symmetry directions, and hence these points must be related to nonsymmetry directions.

Adoption of the Raubenheimer-Gilat method[12] for this model involved, among other things, allowance for complex eigenvectors. The introduction of complex arithmetic slowed the program by a factor of 3. How-ever, at the same time the program was run on the new Oak Ridge IBM 360/91 computer, so that the com-putation time for the calculation of the $g(\nu)$ shown in Fig. 7 was 3 min, as compared to 30 min for the calcu-lations mentioned in Ref. 12, which were carried out on a CDC 1604A computer.

3. Heat capacity and Debye temperature. As mentioned in the Introduction there has recently been considerable interest in the magnetic properties of the rare-earth metals. Various bulk properties of these metals, such as electrical resistance and specific heat, reflect the changes of magnetic structure; often a peak or a knee

will occur in the temperature variation of these proper-ties at the magnetic transitions.

At low temperatures the magnetic contribution C_M to the total specific heat C_P is large in comparison with the electronic C_E, lattice C_L, and nuclear C_N contribu-tions. Recently, Lounasmaa[26] and Lounasmaa and Sundström[27,28] have reported specific-heat measure-ments and analyses for many of the rare-earth metals between 3 and 25°K. In order to analyze the total specific heat into its components, they had to make fairly drastic assumptions concerning the lattice specific heat. As a first approximation, they assumed that both the magnetic and the nonmagnetic heavy rare earths have the same lattice specific heat. In Refs. 27 and 28 this assumption took the form of $C_E(x) + C_L(x) = C_P(Lu)$, where x stands for any of the heavy rare-earth metals and Lu stands for lutetium. Thus, using the expression $C_P(x) = C_N(x) + C_P(Lu) + C_M(x)$, where $C_N(x)$ is taken from low-temperature work,[29] Lounasmaa and Sundström were able to determine the magnetic term $C_M(x)$.

The lattice specific heat, however, may readily be computed in the harmonic approximation from the fre-quency distribution function $g(\nu)$. As an approximation, Sundström[4] used modified axially symmetric models, including up to third nearest neighbors, which were based on single-crystal elastic constant data available for Gd, Er, and Dy, for the calculation of the $g(\nu)$ and the lattice specific for these materials. The dispersion relations calculated from these models show a qualita-tive similarity with our measurements. However, in

[25] L. Van Hove, Phys. Rev. 89, 1189 (1953).

[26] O. V. Lounasmaa, Phys. Rev. 143, 399 (1966).
[27] O. V. Lounasmaa and L. J. Sundström, Phys. Rev. 150, 399 (1966).
[28] O. V. Lounasmaa and L. J. Sundström, Phys. Rev. 158, 591 (1967).
[29] See Ref. 4 and references given there.

view of the necessity of including eight nearest neighbors and zone-boundary data in order to obtain a satisfactory model, it cannot be expected that a good quantitative agreement will exist between the measured dispersion relations and the calculated ones. As a matter of fact, recent measurements[30] of the phonon dispersion relation in Gd (performed on a single crystal of the low absorbant Gd[160]) show a significant difference from the calculated values. This difference, in turn, will be reflected in $g(\nu)$, and it is to be expected that the resulting lattice specific heat will still have a considerable uncertainty, although the lattice specific heat is not very sensitive to the details of the model.

Using the $g(\nu)$ shown in Fig. 7, we have calculated $C_V{}^L$, the lattice specific heat of Tb at constant volume in the harmonic approximation, and the result of this calculation is shown in Fig. 8. In this figure we have also shown C_P for Tb as measured by Jennings et al.[7] Furthermore, we have plotted $C_V{}^L + C_V{}^E$, where $C_V{}^E$ is calculated as $9.5T$ mJ/mole °K.[31] Subtracting $C_V{}^L + C_V{}^E$ from C_P, neglecting C_N, which is of importance only at very low temperatures, and noticing that the difference between C_P and C_V in Tb is negligible, we are left with C_M for Tb. The spike in C_M (or C_P) at ~ 226°K corresponds to the transition from the spiral magnetic phase to the paramagnetic phase. It is interesting to notice that there is a significant magnetic contribution to the specific heat at temperatures appreciably above the transition temperature. There is very good agreement between the measured and calculated specific heat at high temperature.

In Fig. 8 we have also shown by the point at 90°K the result of the calculated total of $C_V{}^L + C_V{}^E + C_M$, where C_M is calculated[2,5] from the frequency distribution function for magnetic excitations at 90°K that was obtained from the measured magnon dispersion relation at this temperature.[32] It is seen that there is extremely good agreement between the measurement and the calculation. This agreement may seem surprising considering that anharmonic effects have been

neglected in the calculation of $C_V{}^L$. However, the melting point for Tb is very high (~ 1330°C) and at the temperatures considered here the anharmonic effects are therefore probably small. At least they would not be expected to have a large effect on the calculated lattice specific heat. Also, it has been shown that similar effects in the magnetic excitations would have only a small effect on C_M at 90°K.[33]

Figure 9 shows the calculated Debye temperature Θ_D. There is a qualitative similarity with the Debye temperature calculated by Sundström[4] for Gd, Dy, and Er. We have relatively good agreement at low temperatures with Rosen's results[34] from measurements of elastic moduli on polycrystalline samples. However, at room temperature Rosen's result is appreciably higher than our calculated values.

IV. SUMMARY

Neutron inelastic scattering measurements of the phonon dispersion relation of terbium metal have been analyzed by means of a Born–von Kármán interatomic force model. The results of this analysis have shown that in order to obtain a satisfactory fit to these data, the model must include both general (tensor) interactions and interactions which extend to the eighth nearest neighbors. The model presented here includes general interactions out to the fourth nearest neighbor and axially symmetric interactions beyond. We emphasize the necessity of including zone-boundary data in the fitting analysis. In this connection, the adequacy of models obtained previously for hexagonal materials[17–20] should be questioned.

The model obtained from this analysis has provided the basis for a calculation of a frequency distribution function for Tb, and this in turn has been used to calculate the lattice specific heat as a function of temperature. At 90°K, where a calculation of the magnetic contribution to the specific heat exists,[5] the total calculated specific heat has been compared with experiment.[7] Excellent agreement between experiment and the calculation is found.

[30] R. M. Nicklow and W. C. Koehler (private communication).

[31] L. D. Jennings, R. E. Miller, and F. H. Spedding, J. Chem. Phys. **33**, 1849 (1960).

[32] H. Bjerrum Møller and J. C. Gylden Houmann, Phys. Rev. Letters **17**, 737 (1966).

[33] M. S. S. Brooks, D. A. Goodings, and H. I. Ralph, J. Phys. C **1**, 1596 (1968).

[34] M. Rosen, Phys. Rev. Letters **19**, 695 (1967).